

# Superfluid vortex dynamics in an elliptical boundary

Matteo Caldara<sup>1,\*</sup>, Andrea Richaud<sup>2</sup>, Pietro Massignan<sup>2,†</sup> and Alexander L. Fetter<sup>3</sup>

**1** Scuola Internazionale Superiore di Studi Avanzati (SISSA), Via Bonomea 265, I-34136, Trieste, Italy

**2** Departament de Física, Universitat Politècnica de Catalunya, Campus Nord B4-B5, E-08034 Barcelona, Spain

**3** Department of Physics and Department of Applied Physics, Stanford University, Stanford, California 94305-4045, USA

\* mcaldara@sissa.it, † pietro.massignan@upc.edu

November 23, 2023

## Abstract

Recent advances in cold atom platforms, providing experimental accessibility to real-time dynamics, have renewed interest in the motion of superfluid vortices in two-dimensional domains. Motivated by this development, we study the dynamics of a vortex in a two-dimensional incompressible superfluid inside an elliptical boundary. Employing the Joukowski conformal map from a circle to an ellipse, we derive an analytical expression for the complex potential describing the hydrodynamic flow around the vortex. We integrate the resulting equations of motion, finding that the vortex moves along a nearly (but not exactly) elliptical trajectory. In addition, we obtain a simple closed expression for the vortex self-energy, which serves as the Hamiltonian of the system.

---

## Contents

<b>1</b>	<b>Introduction</b>	<b>1</b>
<b>2</b>	<b>Joukowski transformation</b>	<b>3</b>
<b>3</b>	<b>Superfluid vortices on an elliptical domain</b>	<b>5</b>
3.1	Complex potential and flow field	5
3.2	Vortex trajectories	9
3.3	Total energy for a single vortex	10
3.4	Comparison with total energy expressed in elliptic coordinates	12
<b>4</b>	<b>Conclusions and outlook</b>	<b>13</b>
	<b>References</b>	<b>14</b>

---

## 1 Introduction

Quantized vortices are fundamental excitations of superfluids, including liquid <sup>4</sup>He-II [1], dilute one- and two-component Bose-Einstein condensates (BECs), and two-component fermionic

mixtures [2, 3]. At low temperatures, these systems become nearly ideal fluids with negligible compressibility, viscosity, and dissipation. As a result, superfluid vortices obey the dynamical equations of classical hydrodynamics [4, 5] augmented with the condition of quantized vorticity [6, 7].

When vortices form in a thin two-dimensional film, their dynamics simplifies greatly because the extra degree of freedom connected to vortex bending freezes out. Hence the point-vortex model applies; it describes a vortex as a point-like object that obeys *first* order equations of motion, with the  $x$  and  $y$  coordinates of each vortex as canonically conjugate variables.

In the 1960s, experiments with rotating superfluid He-II [8, 9] stimulated theoretical studies of equilibrium two-dimensional vortex states in cylinders [10] and annuli [11]. Over the past few years, some of us have studied the dynamics of quantized vortices on nonplanar 2D surfaces, including cylinders [12], cones and planar sectors [13], toroidal surfaces (and their genus-1 generalizations) [14], and ellipsoidal geometries (and their genus-0 generalizations) [15].

These works relied on the complex potential formalism that exploits the properties of conformal transformations. In the following, we briefly review this method, referring to Ref. [13] for a more detailed explanation. It is useful to describe a superfluid system at low temperature with a macroscopic condensate wave function  $\Psi(\mathbf{r}) = \sqrt{n(\mathbf{r})}e^{i\Phi(\mathbf{r})}$  in terms of two real fields, the number density  $n(\mathbf{r})$  and the phase  $\Phi(\mathbf{r})$ . The latter determines the two-dimensional superfluid velocity through  $\mathbf{v} = \hbar\nabla\Phi/M$ , with  $M$  the atomic mass. The flow is then irrotational,  $\nabla \times \mathbf{v} = 0$ , everywhere except at the phase singularities associated with the vortex cores.

Most cold-atom experiments are performed in the Thomas-Fermi (TF) regime [16], where local changes in the density become small. In this case, the continuity equation for particle conservation,  $\partial_t n + \nabla \cdot (n\mathbf{v}) = 0$ , implies that the flow is also incompressible, with  $\nabla \cdot \mathbf{v} = 0$ . As a consequence, a two-dimensional flow may also be described by the stream function  $\chi(\mathbf{r})$ , in terms of which the superfluid velocity in the  $xy$  plane becomes  $\mathbf{v} = (\hbar/M)\hat{\mathbf{z}} \times \nabla\chi$ .

We now have two distinct representations of the hydrodynamic velocity  $\mathbf{v}$ . When written out in detail, the cartesian components of  $\mathbf{v}$  satisfy the Cauchy-Riemann equations. Hence  $\chi$  and  $\Phi$  can be the real and imaginary parts of an analytic function of a complex variable  $z = x + iy$ . In this way, we construct the complex potential defined as

$$F(z) = \chi(\mathbf{r}) + i\Phi(\mathbf{r}), \quad (1)$$

with  $\mathbf{r}$  the two-dimensional position vector. The Cauchy-Riemann conditions give the following compact representation of the hydrodynamic flow velocity:

$$v_y + iv_x = \frac{\hbar}{M} \frac{dF(z)}{dz}. \quad (2)$$

Early experiments on rotating  $^4\text{He-II}$  used circular containers with rotationally invariant walls. For such a geometry, surface roughness at the wall triggers the nucleation of vortices, which then migrate into the bulk of the superfluid. In contrast, a rotating elliptical boundary pushes the superfluid, imparting angular momentum even though the flow remains irrotational for slow rotations. As the rotation rate increases, however, isolated vortices eventually appear within the container [17]. These predictions stimulated experimental studies of vortex states in rotating superfluid  $^4\text{He-II}$  for three elliptical containers with different eccentricities [18]. The results agreed within 10% of theoretical predictions, confirming that the equilibrium of a superfluid rotating at angular velocity  $\Omega$  with angular momentum  $L$  minimizes the free energy  $E - \Omega L$ .

Reference [17] focused on the energy and angular momentum of a vortex in an elliptical boundary, with no consideration of the associated vortex dynamics, which was experimentally inaccessible at that time. More recently, the creation of cold-atom Bose-Einstein condensates (BECs) has allowed direct real-time studies of vortex dynamics [19–21]. In this context,

we study here the motion of two-dimensional superfluid vortices inside a stationary elliptical boundary. An additional motivation is the recent experimental accessibility of such configurations using digital micromirror devices (DMDs) [22–28].

One of us previously used elliptic coordinates to study the energy and angular momentum of a single vortex inside an elliptical boundary, leading to an infinite series [17]. Here, we solve the same problem with a complex potential that yields closed forms for the same quantities. More precisely, we combine earlier results for a single vortex in a planar annulus with the Joukowski transformation to derive the complex potential for a vortex inside an elliptical boundary, from which the dynamics, energy, and angular momentum readily follow.

The complex potential for a single vortex inside a circular boundary needs only a single image vortex outside the boundary. Hence it is natural to consider the possibility of one or more images for a vortex inside an elliptical boundary. In an earlier work [29], Majic used elliptic coordinates to solve the problem of a two-dimensional point charge inside an elliptical conducting boundary, resulting in an infinite set of images outside the boundary. We shall show that our closed form is completely equivalent. As an alternative approach to our combined conformal transformations, Ref. [30] gives a direct transformation from a disk to an ellipse, but it requires complicated analytical expressions that do not seem intuitive.

The paper is organized as follows: Section 2 presents the Joukowski transformation and its analytic properties that play an important role in our analysis. We develop in Sec. 3 the point-vortex model for a single superfluid vortex inside a two-dimensional elliptical boundary. In a planar annulus, a single vortex has a well-studied closed form for its complex potential involving the Jacobi theta function  $\vartheta_1(z)$  [11]. The introduction of the Joukowski map from a circular to an elliptical boundary requires modified boundary conditions that we discuss in detail. In this way, we obtain a closed analytical expression for the complex potential, leading to the equations of motion for a vortex in an elliptical boundary. Their numerical solution gives the vortex trajectories, which are approximately but not exactly elliptic. To conclude the section, we find the self-energy of a single vortex inside an elliptical domain, providing a closed formula for this quantity that Ref. [17] previously expressed as an infinite series. The associated constant-energy curves confirm the nested structure of self-similar approximate ellipses. The resulting Hamiltonian equations of motion agree with those found earlier with the complex potential. Finally, in Sec. 4, we draw conclusions and suggest possible future perspectives of our work.

## 2 Joukowski transformation

The Joukowski transformation [31] usually appears in connection with airfoil design, which can be quite intricate [32]. Here, however, we use its simpler property of mapping concentric circles into a family of confocal ellipses. Combining the Joukowski map (which has the important property of being conformal) with the previous study of a vortex in an annulus [11] is the key to derive our closed form for the complex potential of a vortex in an elliptical boundary.

Consider an elliptical boundary with semiaxes  $a > b$  and focal distance  $c = \sqrt{a^2 - b^2}$ . With no loss of generality, we set  $c = 1$  (meaning that all the lengths are given in terms of  $c$ ) so that  $b = \sqrt{a^2 - 1}$ . In this way, the major semiaxis  $a$  completely specifies the shape of the ellipse.

To describe the two-dimensional superfluid inside an elliptical boundary we use a complex plane parametrized by the coordinate  $w = x + iy$ , with the vortex at the complex position  $w_0 = x_0 + iy_0$ , as shown in the right panel of Fig. 1. The left panel of the same figure shows instead an auxiliary complex plane, defined by the coordinate  $z = X + iY$ .

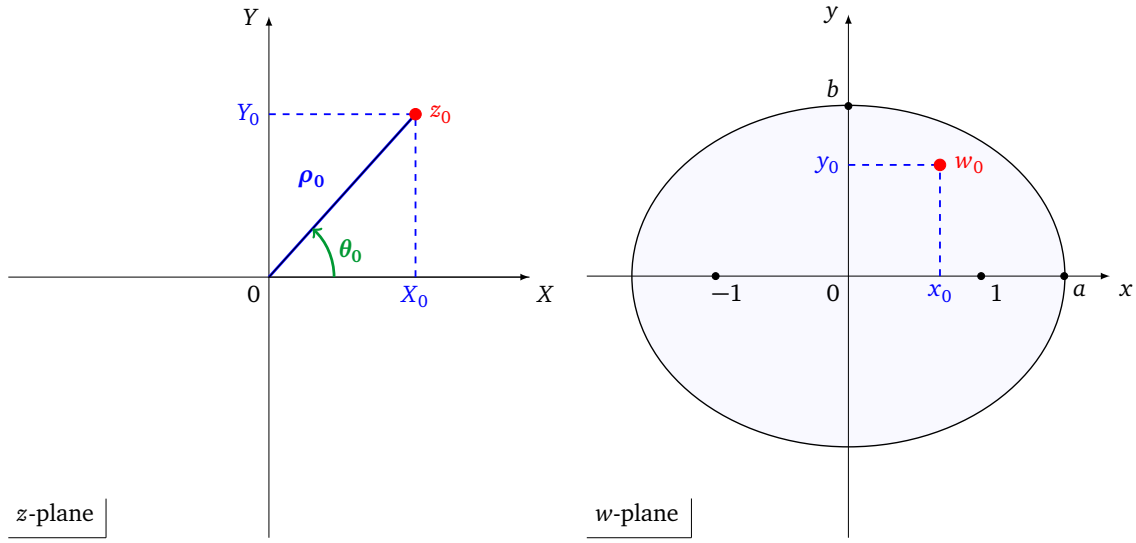


Figure 1: Left: complex  $z$ -plane with a point  $z_0$  specified by both cartesian  $(X_0, Y_0)$  and polar coordinates  $(\rho_0, \theta_0)$ . Right: complex  $w$ -plane with a point  $w_0$ , specified by cartesian coordinates  $(x_0, y_0)$  inside an ellipse with major/minor semi-axes  $a/b$  and focal distance  $c = 1$ .

Consider the Joukowski transformation [31]

$$w = w(z) = \frac{1}{2} \left( z + \frac{1}{z} \right) \quad (3)$$

mapping the  $z$ -plane onto the  $w$ -plane. A transformation is conformal on a given domain if and only if it is analytic, and its derivative is everywhere non-zero. Thus the Joukowski map is conformal on the whole  $z$ -plane, except at the two points  $z = \pm 1$  (because its derivative vanishes there), as well as at  $z = 0$  and  $z \rightarrow \infty$  (where it has simple poles). The action of this map can be understood using polar coordinates for the variable  $z = \rho e^{i\theta}$ , as sketched in the left panel of Fig. 1:

$$x = \frac{\rho + \rho^{-1}}{2} \cos \theta = a \cos \theta, \quad y = \frac{\rho - \rho^{-1}}{2} \sin \theta = b \sin \theta, \quad (4)$$

where  $a = \frac{1}{2}(\rho + \rho^{-1})$  and  $b = \frac{1}{2}(\rho - \rho^{-1})$ , with  $\rho > 1$ . The Joukowski transformation maps a circle of radius  $\rho = a + b = (a - b)^{-1}$  in the region  $|z| > 1$  of the  $z$ -plane into an ellipse in the  $w$ -plane with focal distance  $c = 1$  and semiaxes  $a, b = \sqrt{a^2 - 1}$ . Note that the circle with  $\rho \rightarrow \infty$  maps into a large nearly circular ellipse, whereas the circle with  $\rho \rightarrow 1$  maps onto a closed circuit tightly enclosing the focal line (i.e., a degenerate ellipse with  $a \rightarrow 1$  and  $b \rightarrow 0$ ). In this way, the exterior of the unit circle in the  $z$ -plane maps into the complete  $w$ -plane, apart from the focal line.

The Joukowski map is invariant under the transformation  $z \leftrightarrow z^{-1}$ , which is an inversion in the unit circle. Thus the Joukowski transformation also maps the interior of the unit circle in the  $z$ -plane into the same region in the  $w$ -plane, namely the exterior of the focal line. In particular, the complex point  $1/z_0 = \rho_0^{-1} e^{-i\theta_0}$  also maps into the point  $w_0$ . This inversion symmetry means that the inverse transformation  $z(w)$  is not unique. Instead it is characterized by two distinct branches

$$z = z_{\pm}(w) = w \pm \sqrt{w^2 - 1} \quad (5)$$

that form two Riemann sheets. This structure arises because each disjoint region  $|z| < 1$  and  $|z| > 1$  (inside and outside the unit circle) covers the whole  $w$ -plane. Note that  $z_+(w)z_-(w) = 1$

because of the inversion symmetry. There is a branch cut between  $w = \pm 1$  (i.e., along the focal line of the ellipse) and we define the square root as real along the portion  $x > 1$  of the positive  $x = \text{Re } w$  axis.

We can now make the connection between an annulus in the  $z$ -plane and an ellipse in the  $w$ -plane, which is central in our analysis. Specifically, the vortex dynamics in an annulus is straightforward: the rotational symmetry means that a single vortex precesses uniformly. A combination with the conformal Joukowski transformation readily yields the corresponding vortex dynamics in the interior of an ellipse, even though the rotational symmetry is lost.

We consider a planar annulus with inner and outer radii  $R_1 < R_2$ . It is convenient to use the geometric mean  $\sqrt{R_1 R_2}$  as the length scale, hence we set  $R_2 = R = a + b = a + \sqrt{a^2 - 1} > 1$  and  $R_1 = R^{-1} = a - \sqrt{a^2 - 1} < 1$ . The outer rim  $|z| = R$  transforms into the elliptical boundary, while the circle  $|z| = 1$  maps onto the *flat ellipse* that is a closed loop infinitesimally close to the focal line of the ellipse  $w \in [-1, 1]$ . The inner boundary  $R^{-1}$  of the annulus is the inversion-symmetric partner of the outer annular boundary  $R$ . As can be easily verified, the inner rim  $R^{-1}$  also maps into the elliptical boundary, as expected from the inversion symmetry.

In more detail, the Joukowski transformation may be rewritten as  $2wz = z^2 + 1$ . It is a polynomial of order 1 in  $w$  and of order 2 in  $z$ . Upon traversing the whole  $z$ -plane once, these different powers generate a two-fold covering of the  $w$ -plane. Figure 2 shows the action of the Joukowski conformal map. Each elliptical curve in the  $w$ -plane comes from two circles (identified by the same colour) in the  $z$ -plane: one of them lies in the yellow-shaded  $|z| > 1$  region, and the other lies in the blue-shaded  $|z| < 1$  region. The black outer elliptical boundary corresponds to both the inner and outer rims of the annulus. The two regions in the  $z$ -plane are separated by the black dashed  $|z| = 1$  circle, which maps into the focal line of the ellipse.

It is worth stressing that a single vortex (red dot) at position  $w_0$  in the ellipse is mapped, through the Joukowski transformation, from two same-sign vortices, one in each of the two annular regions. Assuming  $\rho_0 > 1$ , the vortex at position  $z_0 = \rho_0 e^{i\theta_0}$  lies in the yellow  $|z| > 1$  region, whereas the other vortex at  $z_0^{-1} = \rho_0^{-1} e^{-i\theta_0}$  lies inside the blue  $|z| < 1$  region. Moreover, for a fixed polar angle  $\theta_0$ , the two vortices in the annulus lie on the straight lines  $Y(X) = \pm \tan \theta_0 X$ , while for the ellipse they lie on the  $x > 0$  branch of the hyperbola

$$\frac{x^2}{\cos^2 \theta_0} - \frac{y^2}{\sin^2 \theta_0} = 1 \quad (6)$$

in the  $w$ -plane, where we assume  $|\theta_0| < \pi/2$ . These *loci* of points are shown by the brown lines in Fig. 2. Since the Joukowski transformation maps both outer ( $|z| > 1$ ) and inner ( $|z| < 1$ ) regions into the same elliptical region, we can consider only the outer region with  $|z| > 1$  with no loss of generality.

### 3 Superfluid vortices on an elliptical domain

In this section, we combine the complex potential for a single vortex in an annulus [11, 12] with the Joukowski transformation to find the complex potential for a single vortex in an elliptical domain. In doing so, we make use of the following property of conformal transformations between physical flow patterns, as presented in Ref. [33]: “in flow patterns related by a conformal map, circulation integrals around corresponding curves are the same”.

#### 3.1 Complex potential and flow field

Consider a (positive) vortex at position  $w_0$  inside an ellipse with major semiaxis  $a$  and minor semiaxis  $b = \sqrt{a^2 - 1}$ . The dimensionless circulation (in units of  $\hbar/M$ ) around the elliptical boundary is  $\Gamma_{\text{ext}} = +2\pi$ , while the one along the flat ellipse (surrounding the focal line)

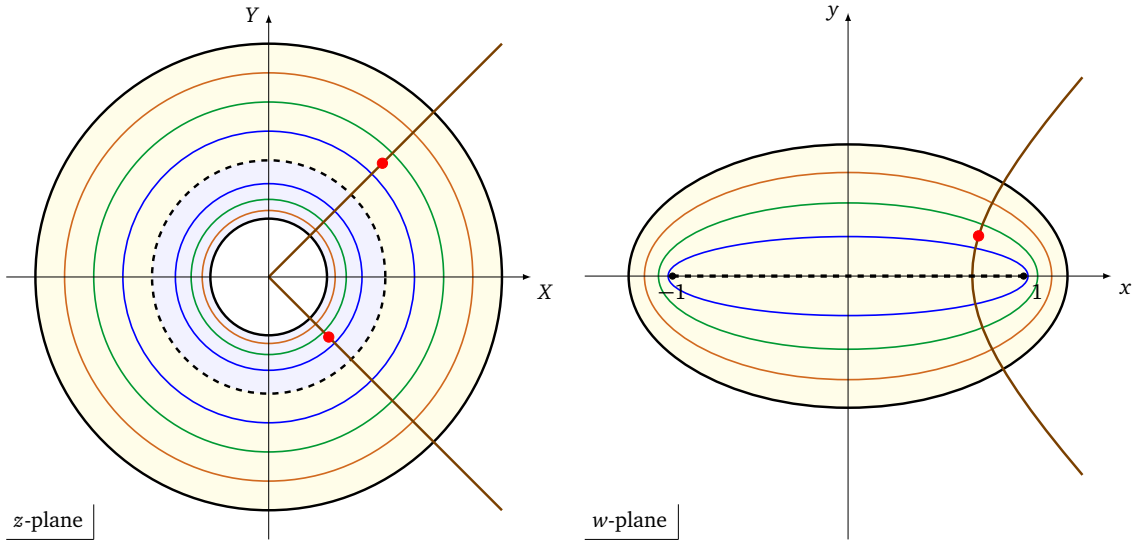


Figure 2: The Joukowski transformation maps concentric circles into confocal ellipses. Curves with the same colour are related by the conformal transformation: the same ellipse comes from two corresponding circles with inverse-symmetric radii. The black-dashed unit circle is mapped into the degenerate flat ellipse surrounding the focal line. Yellow and blue-shaded regions in the left panel represent, respectively, the two Riemann sheets  $|z| > 1$  and  $|z| < 1$  within the annulus: each of these regions maps into the interior of the ellipse in the  $w$ -plane (right panel). Moreover, the Joukowski transformation maps both point vortices at positions  $z_0$  and  $z_0^{-1}$  in the annulus into a single vortex at position  $w_0$  in the ellipse. The *locus* of points with polar coordinates  $\pm\theta_0$  inside the annulus, i.e. a semi-line in the  $z$ -plane, is mapped to a single branch of hyperbola in the  $w$ -plane (brown curves).

is  $\Gamma_{FE} = 0$ . The analogous complex potential on the  $z$ -plane for a vortex in an annulus at  $z_0 = w_0 + \sqrt{w_0^2 - 1}$  must lead to the same circulations along the corresponding boundaries. Hence the complex potential on the  $z$ -plane must feature a circulation  $\Gamma(R) = 2\pi$  on the outer boundary of the annulus (with  $R = a + b$ ) and  $\Gamma(1) = 0$  on the unit circle. Moreover, the flat ellipse in the  $w$ -plane tightly encircles the branch-cut extending between the two foci. To ensure that the flow on the ellipse remains continuous across the branch cut, we must require  $F_{\text{annulus}}(e^{i\theta}) = F_{\text{annulus}}(e^{-i\theta})$  on the unit circle (parametrized by the polar angle  $\theta$ ).

The complex potential for a single (positive) vortex at position  $z_0$  inside an annulus of radii  $R^{-1} < 1 < R$  reads [11, 12]

$$F_{\text{annulus,single}}(z; z_0) = \ln \left[ \frac{\vartheta_1\left(-\frac{i}{2} \ln\left(\frac{z}{z_0}\right), q\right)}{\vartheta_1\left(-\frac{i}{2} \ln\left(\frac{zz_0^*}{R^2}\right), q\right)} \right], \quad (7)$$

where  $\vartheta_1(z, q)$  denotes the first Jacobi theta function, and its *nome*  $q \equiv R_1/R_2 = R^{-2} < 1$  can be rewritten in terms of the parameters of the ellipse as  $q = (a - b)^2$ . In particular, this potential yields a flow with circulation on the outer boundary only: i.e.  $\Gamma(R) = 2\pi$ , and  $\Gamma(R^{-1}) = 0$ .

As we argue below, the correct complex potential in the  $z$ -plane requires an additional term:

$$F_{\text{annulus}}(z; z_0) = F_{\text{annulus,single}}(z; z_0) + F_{\text{annulus,single}}(z^{-1}; z_0). \quad (8)$$

By construction, this potential is symmetric under the exchange  $z \leftrightarrow z^{-1}$ . To understand the physical meaning of this complex potential, we use the quasiperiodicity of the Jacobi  $\vartheta_1$

function<sup>1</sup> to show that (apart for an irrelevant constant) Eq. (8) may be conveniently re-written as

$$F_{\text{annulus}}(z; z_0) = F_{\text{annulus, single}}(z; z_0) + F_{\text{annulus, single}}(z; z_0^{-1}) - \ln(z). \quad (9)$$

The first two terms in the latter equation correspond to the flows generated by a positive vortex at  $z_0$  and by its positive symmetric partner located at  $z_0^{-1}$ . Each of these terms induces  $2\pi$  circulation at the outer boundary  $|z| = R$ , and 0 at the inner one  $|z| = R^{-1}$ . The last term in the equation represents a negative vortex at the origin of the  $z$ -plane, which removes  $2\pi$  circulation everywhere. As a result, the combination of the three terms yields  $\Gamma(R) = 2\pi$  and  $\Gamma(R^{-1}) = -2\pi$ . Furthermore, the unit circle contains two vortices with opposite sign, so that the circulation along it vanishes, namely  $\Gamma(1) = 0$ . This behaviour reflects the built-in symmetry  $z \leftrightarrow z^{-1}$ , ensuring that  $F_{\text{annulus}}(e^{i\theta}) = F_{\text{annulus}}(e^{-i\theta})$ . Summarizing, the complex potential (8) satisfies all the requested conditions [the circulations  $\Gamma(R) = +2\pi$ ,  $\Gamma(1) = 0$  and the symmetry which guarantees continuity across the flat ellipse] in the simply connected region  $1 \leq |z| \leq R$ . In this way, the Joukowski map projects the latter region in a one-to-one fashion onto the whole ellipse, with no ambiguity.

The panels on the left side of Fig. 3 show the stream function  $\chi(\mathbf{r}) = \text{Re} F_{\text{annulus}}(z; z_0)$ , the phase field  $\Phi(\mathbf{r}) = \text{Im} F_{\text{annulus}}(z; z_0)$  and the superfluid velocity field  $\mathbf{v}(\mathbf{r})$  [obtained from Eq. (2)] of this two-vortex configuration on the annulus in the  $z$ -plane.

As a final step, it is convenient to introduce the compact notation

$$\mathfrak{z} \equiv \mathfrak{z}(w) = w + \sqrt{w^2 - 1}, \quad \mathfrak{z}_0 \equiv \mathfrak{z}(w_0). \quad (10)$$

As a result, the complex potential for a single vortex inside the ellipse in the  $w$ -plane has the following analytical expression:

$$\begin{aligned} F_{\text{ellipse}}(w; w_0) &= F_{\text{annulus}}(z(w) = \mathfrak{z}; z_0(w_0) = \mathfrak{z}_0) \\ &= \ln \left[ \frac{\vartheta_1\left(-\frac{i}{2} \ln\left(\frac{\mathfrak{z}}{\mathfrak{z}_0}\right), q\right)}{\vartheta_1\left(-\frac{i}{2} \ln\left(q\mathfrak{z}\mathfrak{z}_0^*\right), q\right)} \right] + \ln \left[ \frac{\vartheta_1\left(-\frac{i}{2} \ln\left(\frac{1}{\mathfrak{z}\mathfrak{z}_0}\right), q\right)}{\vartheta_1\left(-\frac{i}{2} \ln\left(q\frac{\mathfrak{z}_0^*}{\mathfrak{z}}\right), q\right)} \right]. \end{aligned} \quad (11)$$

The result (11) satisfies the correct boundary conditions of the superfluid flow in the  $w$ -plane of the ellipse as it is clear in the panels on the right of Fig. 3, showing the stream function, phase field and superfluid velocity field based on the complex potential (11).

We recall that a single vortex inside an annulus requires an infinite set of image vortices [11] to ensure that the superfluid flow is tangent at both the boundaries. The same situation holds for a single vortex inside an elliptical domain, as it is clear from our previous reasoning, based on the combination of the complex potential for an annulus with the Joukowski transformation. In particular, we have verified that the infinite set of image vortices generated (outside the elliptical container) by Eq. (11) agrees with the set of images found in Ref. [29]. Our derivation, however, seems simpler and more straightforward, since it involves only the three Eqs. (7), (8), and (11).

<sup>1</sup> $\vartheta_1(z \pm \pi\tau, q) = -q^{-1}e^{\mp 2iz}\vartheta_1(z, q)$ , where the parameter  $\tau$  is related to the nome  $q$  by  $q \equiv e^{i\pi\tau}$ .

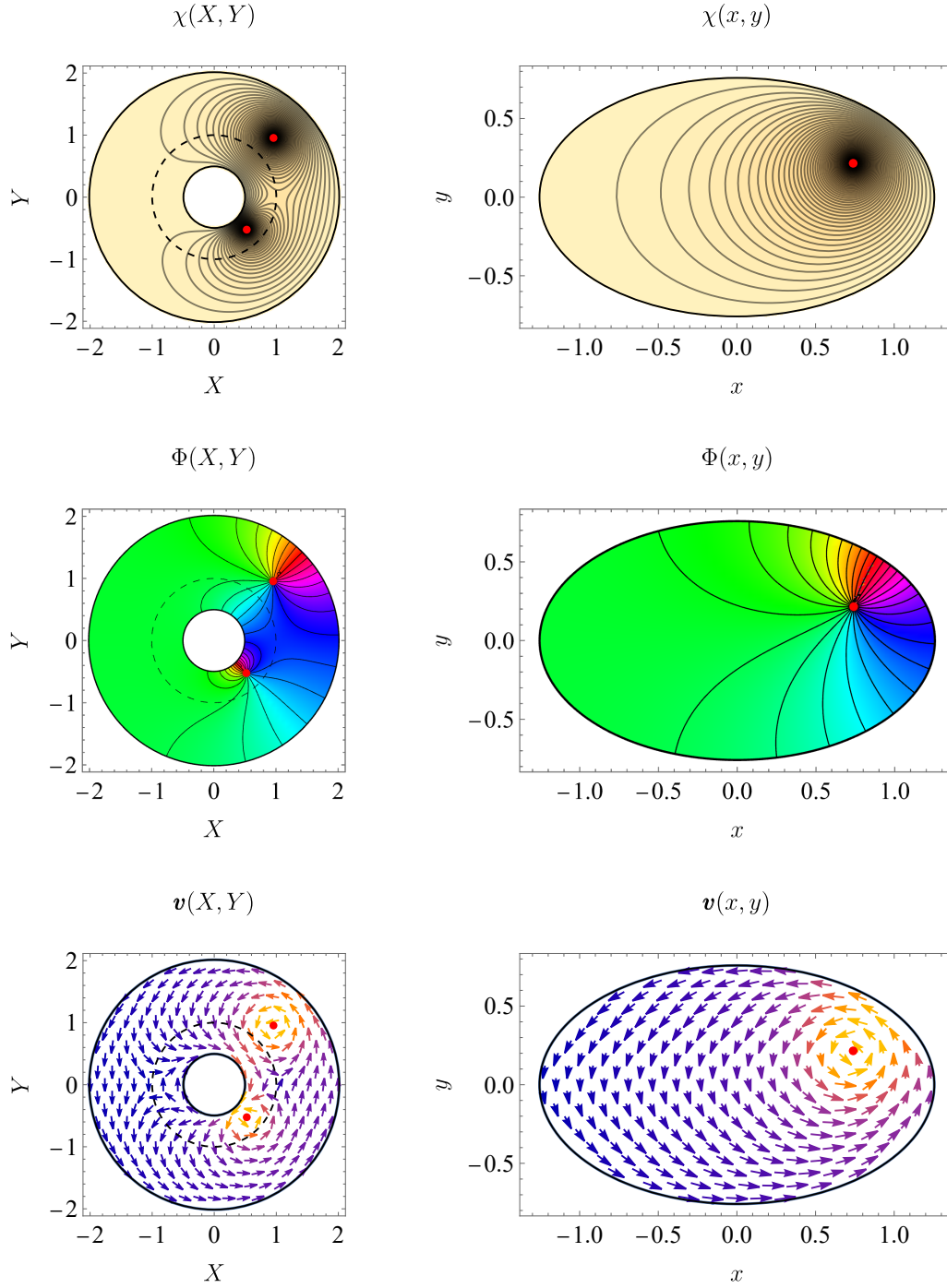


Figure 3: Left column: stream function, phase and velocity field associated with two vortices at positions  $z_0, z_0^{-1}$  inside the planar annulus. The annulus has outer and inner radii  $R = 2, R^{-1} = 1/2$ , the dashed line representing the unit circle. The polar coordinates for the vortex at complex position  $z_0 = \rho_0 e^{i\theta_0}$  are  $\rho_0 = 1.35, \theta_0 = \pi/4$ . Right column: stream function, phase and velocity field associated with a single vortex at  $w_0$  inside the ellipse. The ellipse has eccentricity  $b/a = (R^2 - 1)/(R^2 + 1) = 0.6$ , and the cartesian coordinates of the vortex at position  $w_0$  are  $x_0 \approx 0.74, y_0 \approx 0.22$ .

### 3.2 Vortex trajectories

The velocity of the vortex at position  $z_0$  inside the ellipse follows directly from Eq. (11) as:

$$\begin{aligned}
 i\dot{w}_0^* = \dot{y}_0 + i\dot{x}_0 &= \frac{\hbar}{M} \lim_{w \rightarrow w_0} \left[ F'_{\text{ellipse}}(w; w_0) - \frac{1}{w - w_0} \right] \\
 &= \frac{\hbar}{M} \left\{ -\frac{w_0}{2(w_0^2 - 1)} + \frac{i}{2\sqrt{w_0^2 - 1}} \left[ \frac{\vartheta_1'(i \ln \mathfrak{z}_0, q)}{\vartheta_1(i \ln \mathfrak{z}_0, q)} + \right. \right. \\
 &\quad \left. \left. + \frac{\vartheta_1'(-\frac{i}{2} \ln(q |\mathfrak{z}_0|^2), q)}{\vartheta_1(-\frac{i}{2} \ln(q |\mathfrak{z}_0|^2), q)} - \frac{\vartheta_1'(-\frac{i}{2} \ln(q \frac{\mathfrak{z}_0^*}{\mathfrak{z}_0}, q)}{\vartheta_1(-\frac{i}{2} \ln(q \frac{\mathfrak{z}_0^*}{\mathfrak{z}_0}, q)} \right) \right] \right\}. \tag{12}
 \end{aligned}$$

We integrate the complex dynamical equation (12) to find the closed vortex trajectories for various initial positions along the positive horizontal axis, as shown in Fig. 4. The resulting family clearly differs from the confocal ellipses shown on the right side of Fig. 2. Instead they resemble nested self-similar ellipses. This result is not surprising because the elliptical boundary is a quadrupolar distortion of a circular boundary. Hence the closed trajectories in the elliptical boundary should resemble a family of circles with quadrupolar distortions.

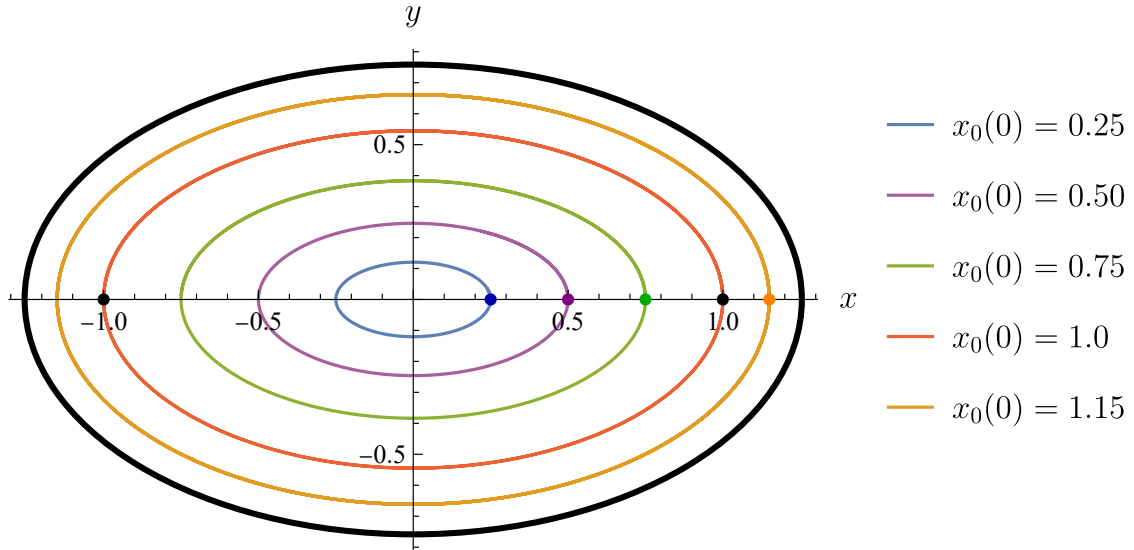


Figure 4: Trajectories of a single vortex inside an elliptical boundary for various initial positions on the positive horizontal axis. The thick black line denotes the outer boundary ( $b/a = 0.6$ ) and the black dots denote the focal points. These trajectories are obtained from numerical solution of the equations of motion (12).

In detail, however, the situation is more complicated. For a circular boundary, the rotational symmetry ensures conservation of angular momentum, so that all vortex trajectories are circles. In contrast, an elliptical boundary does not conserve angular momentum because the boundary is invariant only under a finite rotation by  $\pm\pi$ . If we use an angular Fourier expansion for the trajectory, only even harmonics can occur, and the nonlinear dynamical equations couple the various Fourier amplitudes. As a result, the orbits are not strictly ellipses. More quantitatively, for a given trajectory we extract the maximum value of the coordinates  $(x_{\max}, y_{\max})$  and the period  $T$ . Figure 5 shows  $(x_0/x_{\max})^2 + (y_0/y_{\max})^2$  evaluated along the five closed trajectories in Fig. 4, characterized by  $x_{\max} = 0.25$  (blue curve), 0.50 (purple), 0.75 (green), 1.0 (red), 1.15 (orange). The quantity  $(x_0/x_{\max})^2 + (y_0/y_{\max})^2$  deviates from

the value 1 that it would have for a pure ellipse, displaying a periodic, anharmonic dependence on the polar angle  $\theta_0 \in [0, 2\pi]$ . As follows from its definition, the maximum value of 1 is reached at  $(\pm x_{\max}, 0)$  and  $(0, \pm y_{\max})$ . The minimum value and the corresponding deviation from 1 differ for each case. Starting from the smallest trajectory (blue curve), the amplitude of the oscillation increases (purple and green), until it reaches its maximum for the trajectory with  $x_{\max} = 1$  (red), which is the one passing through the *foci* of the ellipse. Then, for  $1 < x_{\max} < a$  (orange curve), deviations from 1 progressively decrease due to the influence of the elliptic boundary.

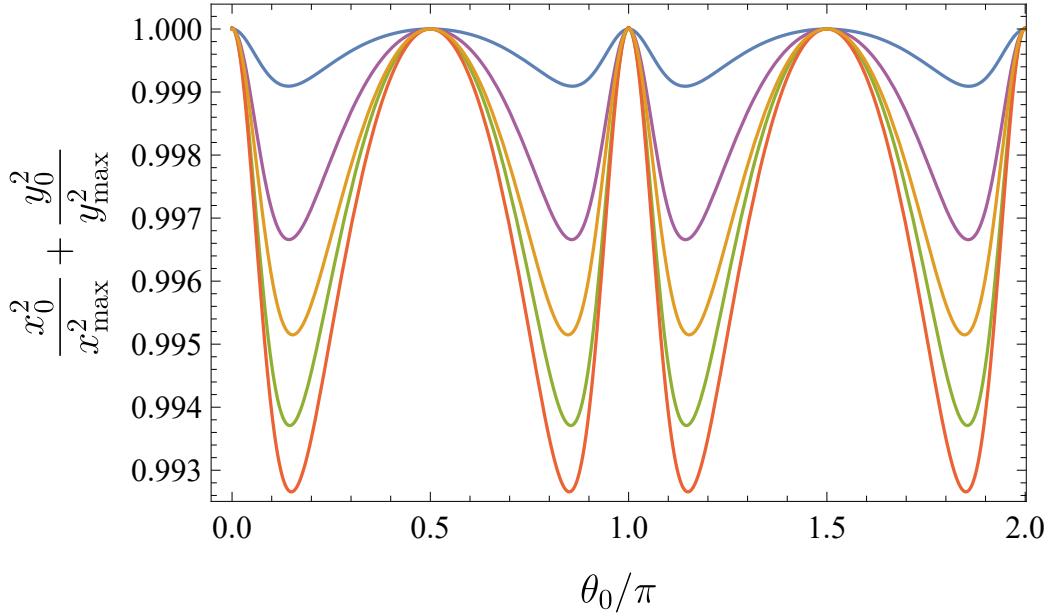


Figure 5: Quantity  $(x_0/x_{\max})^2 + (y_0/y_{\max})^2$  as a function of the polar angle  $\theta_0$  along a closed vortex trajectory. The different curves refer to the five trajectories in Fig. 4, with corresponding colours. Each case shows a periodic deviation from the value 1 that is expected for a pure ellipse.

The numerical evaluation of the period  $T$  for each trajectory then gives the mean precession frequency  $\langle \Omega \rangle = 2\pi/T$ . Figure 6 shows  $\langle \Omega \rangle$  as a function of the initial position along the positive horizontal axis, for three values of the aspect ratio of the container. As the aspect ratio approaches 1, the mean precession frequency converges to the red solid curve, which corresponds to the result for a single vortex inside a disk of radius  $a$ , namely  $\Omega(x_0) = (\hbar/M)(a^2 - x_0^2)^{-1}$ . Importantly, the mean angular velocity is always positive, hence a positive vortex can only move in the counterclockwise direction, independent of its initial position. This result is similar to the circular boundary, while it differs from the case of a vortex inside an annulus, where the precession frequency can be both positive and negative, depending on its position relative to the inner and outer boundaries. Physically, this latter behaviour reflects the influence of the nearest image, which lies beyond the closest boundary.

### 3.3 Total energy for a single vortex

In our model, the energy is purely kinetic, so that the self-energy of the vortex at position  $\mathbf{r}_0 = (x_0, y_0)$  is  $E_0 = \frac{1}{2}nM \int_{\mathcal{E}} d^2r |\mathbf{v}(\mathbf{r})|^2$ , where the integral is restricted to the surface of the elliptical domain  $\mathcal{E} = \{(x, y) \in \mathbb{R}^2 : \frac{x^2}{a^2} + \frac{y^2}{b^2} \leq 1\}$  and  $\mathbf{v}(\mathbf{r}) = (\hbar/M)\hat{\mathbf{z}} \times \nabla\chi(\mathbf{r})$  is the velocity field associated with the vortex in the elliptical boundary. Use the stream function to rewrite

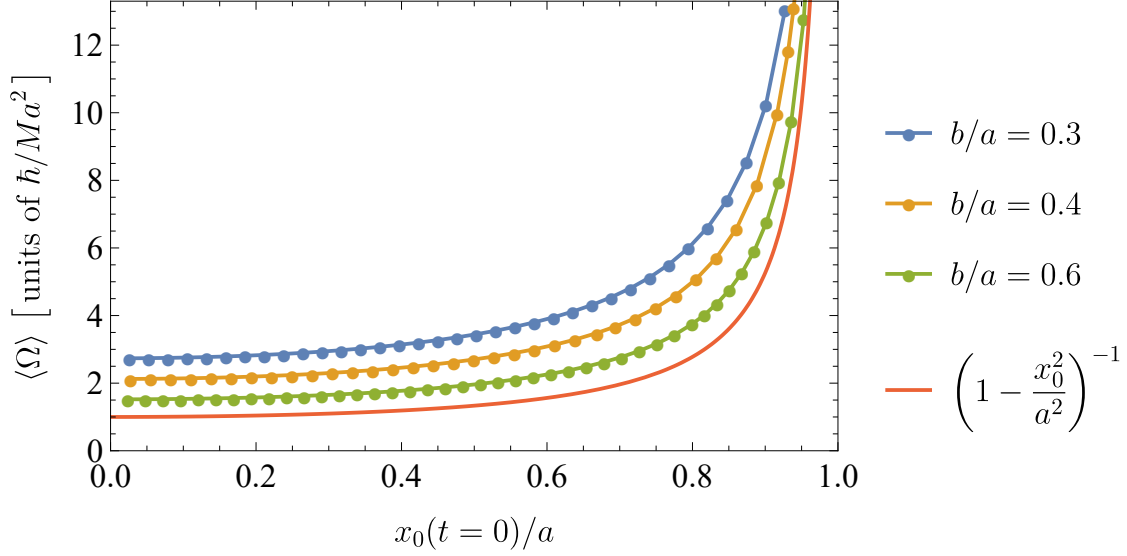


Figure 6: Dependence of the mean precession frequency on the initial position along the positive horizontal axis for three different aspect ratios  $b/a$  of the elliptical boundary. The red solid curve is the result for a circular boundary of radius  $a$ .

the energy as

$$E_0 = \frac{\hbar n}{2} \int_{\mathcal{E}} d^2r \left( -v_x \frac{\partial \chi}{\partial y} + v_y \frac{\partial \chi}{\partial x} \right) = \frac{\hbar n}{2} \left[ \oint_{\partial \mathcal{E}} d\mathbf{l} \cdot \mathbf{v} \chi - \int_{\mathcal{E}} d^2r \chi |\nabla \times \mathbf{v}| \right], \quad (13)$$

where the contour  $\partial \mathcal{E}$  is the elliptical boundary  $\frac{x^2}{a^2} + \frac{y^2}{b^2} = 1$ , taken in the positive sense (counterclockwise). Since the stream function takes the constant value  $\chi(\partial \mathcal{E})$  at the boundary  $\partial \mathcal{E}$  and there is only a single positive vortex inside the ellipse, the line integral is easily evaluated as:

$$\oint_{\partial \mathcal{E}} d\mathbf{l} \cdot \mathbf{v} \chi = \frac{2\pi\hbar}{M} \chi(\partial \mathcal{E}). \quad (14)$$

The remaining surface integral depends on a specific model for the vortex core, described as a circle of radius  $a_c$ . It can be decomposed as follows:

$$\int_{\mathcal{E}} d^2r \zeta \chi = \int_{\mathcal{E}} d^2r \zeta (\chi - \chi_0) + \int_{\text{core}} d^2r \zeta \chi_0, \quad (15)$$

where  $\zeta = |\nabla \times \mathbf{v}| = (2\pi\hbar/M)\delta^{(2)}(\mathbf{r} - \mathbf{r}_0)$  is the vorticity and  $\chi_0 = \ln(|\mathbf{r} - \mathbf{r}_0|/a_c)$ . For simplicity, we assume an empty core surrounded by irrotational flow for  $r > a_c$ , so that the second term in Eq. (15) vanishes. By construction, the regularized stream function  $\chi_{\text{reg}} = \chi - \chi_0$  in the first term is bounded near the vortex core. In this way, Eq. (15) becomes

$$\int_{\mathcal{E}} d^2r \zeta \chi = \frac{2\pi\hbar}{M} \lim_{r \rightarrow r_0} \left[ \chi(r) - \ln\left(\frac{|\mathbf{r} - \mathbf{r}_0|}{a_c}\right) \right] \equiv \frac{2\pi\hbar}{M} \chi_{\text{reg}}(\mathbf{r}_0). \quad (16)$$

A combination of Eqs. (14) and (16) leads to the following form for the self-energy:

$$E_0(\mathbf{r}_0) = \frac{\pi\hbar^2 n}{M} [\chi(\partial \mathcal{E}) - \chi_{\text{reg}}(\mathbf{r}_0)]. \quad (17)$$

The boundary term  $\chi(\partial \mathcal{E})$  is nothing but the real part of the complex potential (8) evaluated at the elliptic boundary: the latter is parametrized by  $x = a \cos \theta$ ,  $y = b \sin \theta$ , with  $\theta = [-\pi, \pi]$ .

Exploiting the definition and properties of elliptic theta functions [34], the constant boundary value of the stream function turns out to be:

$$\chi(\partial\mathcal{E}) = \text{Re} \left[ F_{\text{ellipse}}^{\partial\mathcal{E}}(\theta; w_0) \right] = \frac{1}{2} \ln(q |\mathfrak{z}_0|^2) \Big|_{w_0=x_0+iy_0}. \quad (18)$$

The regularized stream function can be computed as:

$$\begin{aligned} \chi_{\text{reg}}(\mathbf{r}_0) &= \text{Re} \left\{ \lim_{w \rightarrow w_0} \left[ F_{\text{ellipse}}(w; w_0) - \ln \left( \frac{w - w_0}{a_c} \right) \right] \right\} \Big|_{w_0=x_0+iy_0} \\ &= -\ln \left( \frac{2 \vartheta_1 \left( -\frac{i}{2} \ln(q |\mathfrak{z}_0|^2), q \right)}{i a_c \vartheta_1'(0, q)} \right) - \text{Re} \left[ \ln \left( \sqrt{w_0^2 - 1} \frac{\vartheta_1 \left( -\frac{i}{2} \ln \left( q \frac{\mathfrak{z}_0^*}{\mathfrak{z}_0} \right), q \right)}{\vartheta_1(i \ln \mathfrak{z}_0, q)} \right) \right]. \end{aligned} \quad (19)$$

The derivation here is quite intricate and we skip it since it provides little physical insight. Inserting the results (18) and (19) into Eq. (17), and omitting an irrelevant additive constant  $-\ln(2a_c\sqrt{q})$ , the final self-energy in cartesian coordinates becomes:

$$\frac{E_0(x_0, y_0)}{\pi \hbar^2 n/M} = \ln \left[ \frac{4q |\mathfrak{z}_0| \vartheta_1 \left( -\frac{i}{2} \ln(q |\mathfrak{z}_0|^2), q \right)}{i \vartheta_1'(0, q)} \right] + \text{Re} \ln \left[ \sqrt{w_0^2 - 1} \frac{\vartheta_1 \left( -\frac{i}{2} \ln \left( q \frac{\mathfrak{z}_0^*}{\mathfrak{z}_0} \right), q \right)}{\vartheta_1(i \ln \mathfrak{z}_0, q)} \right]. \quad (20)$$

Since our system conserves energy, the associated vortex dynamics obeys Hamilton's equations. Hence the trajectories shown in Fig. 4 are curves of constant energy.

### 3.4 Comparison with total energy expressed in elliptic coordinates

Reference [17] introduced elliptic coordinates  $(\xi, \eta)$  with a conformal transformation  $w = \cosh \zeta$  where  $w = x + iy$  and  $\zeta = \xi + i\eta$ . In this way, we have

$$x = \cosh \xi \cos \eta, \quad y = \sinh \xi \sin \eta, \quad (21)$$

with  $\xi \geq 0$ ,  $-\pi \leq \eta < \pi$ . The elliptical domain, in particular, is obtained for  $0 \leq \xi \leq \Xi$ , with  $\tanh \Xi = b/a$ . A comparison with Eq. (4) shows that the elliptic coordinate  $\eta$  is the same as the polar angle  $\theta$  used for the annulus: in the following we simply replace  $\eta$  with  $\theta$ .

A straightforward extension of results in [17] gives the self-energy for a vortex with elliptic coordinates  $(\xi_0, \theta_0)$

$$\frac{E_0(\xi_0, \theta_0)}{\pi \hbar^2 n/M} = -2 \sum_{m=1}^{\infty} \frac{e^{-m\Xi}}{m} \left( \frac{\cosh^2 m \xi_0 \cos^2 m \theta_0}{\cosh m \Xi} + \frac{\sinh^2 m \xi_0 \sin^2 m \theta_0}{\sinh m \Xi} \right). \quad (22)$$

Here, the energy appears as an infinite series involving both hyperbolic and trigonometric functions. Although less compact than Eq. (20) expressed in terms of the Jacobian theta function  $\vartheta_1$  in cartesian coordinates, it provides some valuable insights.

For example, Hamilton's equations evaluated with the above energy in elliptic coordinates yield the equations of motion for a single vortex, again involving infinite summations

$$\begin{aligned} \dot{\xi}_0 &= \frac{1}{h_0^2} \frac{\partial [E_0/2\pi \hbar n]}{\partial \theta_0} = \frac{\hbar}{M h_0^2} \sum_{m=1}^{\infty} e^{-m\Xi} \sin(2m\theta_0) \left( \frac{\cosh^2 m \xi_0}{\cosh m \Xi} - \frac{\sinh^2 m \xi_0}{\sinh m \Xi} \right), \\ \dot{\theta}_0 &= -\frac{1}{h_0^2} \frac{\partial [E_0/2\pi \hbar n]}{\partial \xi_0} = \frac{\hbar}{M h_0^2} \sum_{m=1}^{\infty} e^{-m\Xi} \sinh(2m\xi_0) \left( \frac{\cos^2 m \theta_0}{\cosh m \Xi} + \frac{\sin^2 m \theta_0}{\sinh m \Xi} \right), \end{aligned} \quad (23)$$

with the metric factor:

$$h_0(\xi_0, \theta_0) = \sqrt{\sinh^2 \xi_0 + \sin^2 \theta_0}. \quad (24)$$

We see immediately that  $\dot{\theta}_0$  is necessarily positive, which means that the vortex always moves in the positive (counterclockwise) direction. The “radial” velocity  $\dot{\xi}_0(t)$  involves a sum over trigonometric functions  $\sin 2m\theta_0$  that are periodic over a half cycle of  $\theta_0$ . In contrast, the second factor in large parentheses is a positive-definite combination of hyperbolic functions. As a result,  $\xi_0(t)$  exhibits periodic but anharmonic oscillations along the orbit. Note that a constant  $\xi_0$  represents a confocal ellipse, as shown on the right side of Fig. 2. The periodic oscillations in  $\xi_0(t)$  modify the trajectories to the nested self-similar form seen in Fig. 4.

Equation (20) gives a closed form for the energy, expressed in complex cartesian coordinates  $w = x + iy$ . Substitution of the conformal transformation  $w = \cosh \zeta$  then gives a closed form for the energy expressed in elliptic coordinates, which we do not write here. A detailed analysis using the infinite product representation of the various  $\vartheta$  functions eventually shows that the two expressions are equivalent.

## 4 Conclusions and outlook

An earlier paper by one of us [17] studied the low-lying equilibrium states of rotating superfluid He-II in an elliptical cylinder. For slow rotations, the rotating walls push the fluid inducing pure irrotational flow. Above a critical angular velocity, however, a vortex appears at the centre of the ellipse. The corresponding predictions for energy and angular momentum found clear confirmation in subsequent experiments [18] for elliptic containers with three different eccentricities.

The present work goes further, investigating the superfluid dynamics of a single vortex in a stationary elliptical boundary. We followed the standard mathematical approach using a complex potential that captures all the physical properties of the superfluid flow. An ellipse is a quadrupolar deformation of a circle, hence one might expect similarities to the familiar case of a vortex in a circular boundary, which requires only a single image to construct the complex potential. In fact, the situation is more intricate. We use the Joukowski transformation that maps concentric circles into confocal ellipses. A thorough analysis of its analytical structure showed that this conformal map links an annulus and an elliptical domain. As a result, we relied on an earlier study of a single vortex in an annulus [11], where the complex potential involves an infinite set of image vortices.

A combination of the conformal Joukowski transformation and the appropriate values for the circulation around both annular boundaries eventually gave Eq. (11) as the final complex potential for the single vortex in an ellipse. The resulting superfluid flow, as shown in Fig. 3, manifestly satisfies all the relevant boundary conditions. Moreover, a detailed study shows that our very compact result agrees with the potential generated by the infinite set of image vortices presented in a previous work in the field of electrostatics [29].

We then used the complex potential to study the resulting vortex dynamics. We integrated the equations of motion for various initial positions to find the closed trajectories that are shown in Fig. 4. Unlike the confocal ellipses associated with the Joukowski transformation, these trajectories form self-similar nearly elliptical orbits. Furthermore, Fig. 6 confirms that all the trajectories have the same positive sense, similar to the motion in a circular boundary, but different from that in an annulus.

Finally, we derived a closed formula in Eq. (20) for the self energy of a vortex in an elliptical boundary. As expected for a Hamiltonian system, the contour lines of this energy coincide with the vortex trajectories found previously by direct integration of the dynamical equations for

the vortex. In addition, a generalization of Ref. [17] based on elliptic coordinates provided an independent numerical confirmation of our results.

As a future extension of this work, one could investigate how a finite massive core affects the vortex dynamics. The time-dependent variational Lagrangian method successfully described massive vortices in a disk [35–37] and in an annulus [38]. In this situation, the mass plays the role of a singular perturbation, since it breaks the familiar structure of first-order dynamical equations of motion for massless vortices. Instead, the dynamical equations for massive vortices become second order in time. Similar to electromagnetic problems, the mass here is responsible for a cyclotron motion superimposed on the drift of a guiding centre. There is also an upper bound for the mass filling the vortex cores, beyond which the trajectories become unstable. It would be interesting to verify that a massive vortex in an elliptical boundary exhibits similar behaviour. Another natural extension of our research would be to study vortex lattices in elliptical containers, and their normal modes and instabilities.

## Acknowledgements

**Funding information** A. R. received funding from the European Union’s Horizon research and innovation programme under the Marie Skłodowska-Curie grant agreement *Vortexons* (no. 101062887). P. M. and A. R. acknowledge support by the Spanish Ministerio de Ciencia e Innovación (MCIN/AEI/10.13039/501100011033, grant PID2020-113565GB-C21), and by the Generalitat de Catalunya (grant 2021 SGR 01411). P. M. further acknowledges support by the *ICREA Academia* program.

## References

- [1] R. J. Donnelly, *Quantized Vortices in Helium II*, Cambridge University Press, Cambridge, ISBN 0521324009 (1991).
- [2] C. J. Pethick and H. Smith, *Bose-Einstein Condensation in Dilute Gases*, Cambridge University Press, Cambridge, 2 edn., doi:[10.1017/CBO9780511802850](https://doi.org/10.1017/CBO9780511802850) (2008).
- [3] S. Stringari and L. Pitaevskii, *Bose-Einstein condensation and superfluidity*, Oxford Science Publications, Oxford, ISBN 9780198758884 (2016).
- [4] G. R. Kirchhoff, *Vorlesungen über Mathematische Physik, Bd. 1: Mechanik*, Teubner, Leipzig (1876).
- [5] H. Lamb, *Hydrodynamics*, chap. 7, Dover, New York, 6th edn., ISBN 0486602567 (1945).
- [6] L. Onsager, *Il Nuovo Cimento* **6** (Suppl. 2), 249 (1949), doi:[10.1007/BF02780988](https://doi.org/10.1007/BF02780988).
- [7] R. P. Feynman, *Application of Quantum Mechanics to Liquid Helium*, In *Progress in Low Temperature Physics*, vol. 1, pp. 17–53. Elsevier, North-Holland, Amsterdam, doi:[10.1016/S0079-6417\(08\)60077-3](https://doi.org/10.1016/S0079-6417(08)60077-3) (1955).
- [8] W. F. Vinen, *The detection of single quanta of circulation in liquid helium II*, *Proceedings of the Royal Society of London. Series A. Mathematical and Physical Sciences* **260**(1301), 218 (1961), doi:[10.1098/rspa.1961.0029](https://doi.org/10.1098/rspa.1961.0029).
- [9] P. J. Bendt and R. J. Donnelly, *Threshold for Superfluid Vortex Lines in a Rotating Annulus*, *Phys. Rev. Lett.* **19**, 214 (1967), doi:[10.1103/PhysRevLett.19.214](https://doi.org/10.1103/PhysRevLett.19.214).

- [10] G. B. Hess, *Angular Momentum of Superfluid Helium in a Rotating Cylinder*, Phys. Rev. **161**, 189 (1967), doi:[10.1103/PhysRev.161.189](https://doi.org/10.1103/PhysRev.161.189).
- [11] A. L. Fetter, *Low-Lying Superfluid States in a Rotating Annulus*, Phys. Rev. **153**, 285 (1967), doi:[10.1103/PhysRev.153.285](https://doi.org/10.1103/PhysRev.153.285).
- [12] N.-E. Guenther, P. Massignan and A. L. Fetter, *Quantized superfluid vortex dynamics on cylindrical surfaces and planar annuli*, Phys. Rev. A **96**, 063608 (2017), doi:[10.1103/PhysRevA.96.063608](https://doi.org/10.1103/PhysRevA.96.063608).
- [13] P. Massignan and A. L. Fetter, *Superfluid vortex dynamics on planar sectors and cones*, Phys. Rev. A **99**, 063602 (2019), doi:[10.1103/PhysRevA.99.063602](https://doi.org/10.1103/PhysRevA.99.063602).
- [14] N.-E. Guenther, P. Massignan and A. L. Fetter, *Superfluid vortex dynamics on a torus and other toroidal surfaces of revolution*, Phys. Rev. A **101**, 053606 (2020), doi:[10.1103/PhysRevA.101.053606](https://doi.org/10.1103/PhysRevA.101.053606).
- [15] M. A. Caracanhas, P. Massignan and A. L. Fetter, *Superfluid vortex dynamics on an ellipsoid and other surfaces of revolution*, Phys. Rev. A **105**, 023307 (2022), doi:[10.1103/PhysRevA.105.023307](https://doi.org/10.1103/PhysRevA.105.023307).
- [16] G. Baym and C. J. Pethick, *Ground-State Properties of Magnetically Trapped Bose-Condensed Rubidium Gas*, Phys. Rev. Lett. **76**, 6 (1996), doi:[10.1103/PhysRevLett.76.6](https://doi.org/10.1103/PhysRevLett.76.6).
- [17] A. L. Fetter, *Vortex nucleation in deformed rotating cylinders*, Journal of Low Temperature Physics **16**, 533 (1974), doi:[10.1007/BF00654901](https://doi.org/10.1007/BF00654901).
- [18] K. DeConde and R. E. Packard, *Measurement of Equilibrium Critical Velocities for Vortex Formation in Superfluid Helium*, Phys. Rev. Lett. **35**, 732 (1975), doi:[10.1103/PhysRevLett.35.732](https://doi.org/10.1103/PhysRevLett.35.732).
- [19] D. V. Freilich, D. M. Bianchi, A. M. Kaufman, T. K. Langin and D. S. Hall, *Real-Time Dynamics of Single Vortex Lines and Vortex Dipoles in a Bose-Einstein Condensate*, Science **329**(5996), 1182 (2010), doi:[10.1126/science.1191224](https://doi.org/10.1126/science.1191224).
- [20] S. Serafini, M. Barbiero, M. Debortoli, S. Donadello, F. Larcher, F. Dalfovo, G. Lamporesi and G. Ferrari, *Dynamics and Interaction of Vortex Lines in an Elongated Bose-Einstein Condensate*, Phys. Rev. Lett. **115**, 170402 (2015), doi:[10.1103/PhysRevLett.115.170402](https://doi.org/10.1103/PhysRevLett.115.170402).
- [21] S. Serafini, L. Galantucci, E. Iseni, T. Bienaimé, R. N. Bisset, C. F. Barenghi, F. Dalfovo, G. Lamporesi and G. Ferrari, *Vortex Reconnections and Rebounds in Trapped Atomic Bose-Einstein Condensates*, Phys. Rev. X **7**, 021031 (2017), doi:[10.1103/PhysRevX.7.021031](https://doi.org/10.1103/PhysRevX.7.021031).
- [22] G. Del Pace, K. Khani, A. Muzi Falconi, M. Fedrizzi, N. Grani, D. Hernandez Rajkov, M. Inguscio, F. Scazza, W. J. Kwon and G. Roati, *Imprinting Persistent Currents in Tunable Fermionic Rings*, Phys. Rev. X **12**, 041037 (2022), doi:[10.1103/PhysRevX.12.041037](https://doi.org/10.1103/PhysRevX.12.041037).
- [23] D. Hernandez-Rajkov, N. Grani, F. Scazza, G. D. Pace, W. J. Kwon, M. Inguscio, K. Khani, C. Fort, M. Modugno, F. Marino and G. Roati, *Universality of the superfluid Kelvin-Helmholtz instability by single-vortex tracking*, arXiv:2303.12631 (2023), doi:[10.48550/arXiv.2303.12631](https://doi.org/10.48550/arXiv.2303.12631).
- [24] K. Khani, G. D. Pace, F. Scazza and G. Roati, *Decay of persistent currents in annular atomic superfluids*, arXiv:2306.11645 (2023), doi:[10.48550/arXiv.2306.11645](https://doi.org/10.48550/arXiv.2306.11645).

- [25] G. Martirosyan, C. J. Ho, J. Etrych, Y. Zhang, A. Cao, Z. Hadzibabic and C. Eigen, *Observation of subdiffusive dynamic scaling in a driven and disordered box-trapped Bose gas*, arXiv:2304.06697 (2023), doi:[10.48550/arXiv.2304.06697](https://doi.org/10.48550/arXiv.2304.06697).
- [26] N. Navon, R. P. Smith and Z. Hadzibabic, *Quantum gases in optical boxes*, Nature Physics **17**(12), 1334 (2021), doi:[10.1038/s41567-021-01403-z](https://doi.org/10.1038/s41567-021-01403-z).
- [27] G. Gauthier, I. Lenton, N. McKay Parry, M. Baker, M. J. Davis, H. Rubinsztein-Dunlop and T. W. Neely, *Direct imaging of a digital-micromirror device for configurable microscopic optical potentials*, Optica **3**(10), 1136 (2016), doi:[10.1364/OPTICA.3.001136](https://doi.org/10.1364/OPTICA.3.001136).
- [28] Y.-Q. Zou, E. Le Cerf, B. Bakkali-Hassani, C. Maury, G. Chauveau, P. C. M. Castilho, R. Saint-Jalm, S. Nascimbene, J. Dalibard and J. Beugnon, *Optical control of the density and spin spatial profiles of a planar Bose gas*, Journal of Physics B: Atomic, Molecular and Optical Physics **54**(8), 08LT01 (2021), doi:[10.1088/1361-6455/abf298](https://doi.org/10.1088/1361-6455/abf298).
- [29] M. Majic, *Images of point charges in conducting ellipses and prolate spheroids*, Journal of Mathematical Physics **62**(9) (2021), doi:[10.1063/5.0054384](https://doi.org/10.1063/5.0054384).
- [30] H. Eskandari, M. S. Majedi, A. R. Attari and Q.-T. Oscar, *Elliptical generalized Maxwell fish-eye lens using conformal mapping*, New J. Phys. **21**(6), 063010 (2019), doi:[0.1088/1367-2630/ab2471](https://doi.org/10.1088/1367-2630/ab2471).
- [31] N. Joukowski, *Über die konturen der tragflächen der drachenflieger*, Zeitschrift für Flugtechnik und Motorluftschiffahrt **1**(22), 281 (1910).
- [32] G. F. Carrier, M. Krook and C. E. Pearson, *Functions of a Complex Variable; Theory and Technique*, sec. 4.5, McGraw-Hill (1966).
- [33] A. M. Turner, V. Vitelli and D. R. Nelson, *Vortices on curved surfaces*, Rev. Mod. Phys. **82**, 1301 (2010), doi:[10.1103/RevModPhys.82.1301](https://doi.org/10.1103/RevModPhys.82.1301).
- [34] E. T. Whittaker and G. N. Watson, *A Course of Modern Analysis*, chap. XXI, Cambridge University Press, Cambridge, UK, 5th edn., doi:[10.1017/9781009004091](https://doi.org/10.1017/9781009004091) (2021).
- [35] A. Richaud, V. Penna, R. Mayol and M. Guilleumas, *Vortices with massive cores in a binary mixture of Bose-Einstein condensates*, Phys. Rev. A **101**, 013630 (2020), doi:[10.1103/PhysRevA.101.013630](https://doi.org/10.1103/PhysRevA.101.013630).
- [36] A. Richaud, V. Penna and A. L. Fetter, *Dynamics of massive point vortices in a binary mixture of Bose-Einstein condensates*, Phys. Rev. A **103**, 023311 (2021), doi:[10.1103/PhysRevA.103.023311](https://doi.org/10.1103/PhysRevA.103.023311).
- [37] A. Richaud, P. Massignan, V. Penna and A. L. Fetter, *Dynamics of a massive superfluid vortex in  $r^k$  confining potentials*, Phys. Rev. A **106**, 063307 (2022), doi:[10.1103/PhysRevA.106.063307](https://doi.org/10.1103/PhysRevA.106.063307).
- [38] M. Caldara, A. Richaud, M. Capone and P. Massignan, *Massive superfluid vortices and vortex necklaces on a planar annulus*, SciPost Phys. **15**, 057 (2023), doi:[10.21468/SciPostPhys.15.2.057](https://doi.org/10.21468/SciPostPhys.15.2.057).